Available online at www.sciencedirect.com
SCIENCE DIRECT
Journal of Molecular Catalysis A: Chemical 245 (2006) 55–61
JOURNAL OF MOLECULAR CATALYSIS A: CHEMICAL
www.elsevier.com/locate/molcata

Effect of M ion oxidation state in $Sr_{1-x}M_xTiO_{3\pm\delta}$ perovskites in methane catalytic flameless combustion

C. Oliva [a,*], S. Cappelli [a], I. Rossetti [a], A. Kryukov [b], L. Bonoldi [c], L. Forni [a]

[a] *Department of Physical Chemistry and Electrochemistry, University of Milan, via Golgi 19, 20133 Milan, Italy*
[b] *D.I. Mendeleev University of Chemical Technology of Russia, Moscow, Russia*
[c] *Polimeri Europa, Novara, Italy*

Received 15 July 2005; received in revised form 26 September 2005; accepted 26 September 2005
Available online 27 October 2005

Abstract

$Sr_{1-x}M_xTiO_{3\pm\delta}$ ($x = 0$ or 0.1; M = K or Gd) have been compared as catalysts for the flameless combustion of methane. The samples were prepared both by traditional sol–gel (SG) and by flame-hydrolysis (FH) procedure. All the catalysts possessed the perovskite-like structure, with some $SrCO_3$ as impurity with $Sr_{0.9}K_{0.1}TiO_{3\pm\delta}$ prepared by SG procedure. All the samples prepared by FH were better catalysts than those prepared by SG. A further improvement in the catalytic activity was obtained with M = K, but only at temperatures lower than 550 °C. X-band and Q-band EPR spectroscopies provided an explanation of this observation, based on the high mobility of surface O_3^- species on the surface of the (FH) $Sr_{0.9}K_{0.1}TiO_{3\pm\delta}$ sample.

Keywords: $SrKTiO_3$ and $SrGdTiO_3$ oxidation catalysts; X-band and Q-band EPR; Flame-hydrolysis preparation technique; Oxygen-centred radicals

1. Introduction

Transition metal oxide mixtures with perovskite-like structure are well-known catalysts for the catalytic flameless combustion (CFC) of methane. The well-known sol–gel-citrate (SGC) procedure [1] allows to obtain a relatively high surface area and hence a better initial activity. However, the relatively low final calcination temperature (usually less than 700 °C) attained with this procedure leads to a thermally poor resistant material. Both these properties, thermal stability and high surface area, can be achieved by preparing the material in nano-size particles, calcined at very high temperature. An innovative preparation method of this kind has been recently proposed [2], based on flame-hydrolysis (FH) of aqueous solutions of precursor salts. In a previous work [3], three samples of $SrTiO_{3\pm\delta}$ have been compared as catalysts for the CFC of methane, to investigate the influence of the different preparation parameters on their catalytic properties. It was found that the presence of paramagnetic species like M^+/O^- ($M^+ = Ti^{4+}$ or Sr^{2+}) and Ti^{4+}/O_3^- is crucial for a good catalytic performance. In the present work, four samples of $SrTiO_{3\pm\delta}$ partially substituted with potassium ($Sr_{0.9}K_{0.1}TiO_{3\pm\delta}$ (KFH) and $Sr_{0.9}K_{0.1}TiO_{3\pm\delta}$ (KSG)) or gadolinium ($Sr_{0.9}Gd_{0.1}TiO_{3\pm\delta}$ (GFH) and $Sr_{0.9}Gd_{0.1}TiO_{3\pm\delta}$ (GSG)) for strontium have been investigated. Two of them (KFH and GFH) were prepared by FH, the other two (KSG and GSG) by the SGC technique. Potassium and gadolinium have been selected because K^+ and Gd^{3+} possess ionic radius close to that of Sr^{2+} [4] and, therefore, they can be easily hosted in the Sr-titanate perovskitic crystal lattice without strong distortions in it. Moreover, the different ionic charge of potassium (1+) and gadolinium (3+) with respect to strontium (2+) induces a non-stoichiometric oxygen composition, which can affect the catalytic activity. Indeed, it has been reported [5] that partial substitution of K for La in $La_{0.9}K_{0.1}Cr_{0.9}O_{3-\delta}$ reduces the catalytic activity for CFC of methane, while increases the catalytic activity for soot combustion, e.g. for abatement of polluting particulate coming from diesel engines. This behaviour was accounted for by hypothesizing the presence, in that catalyst, of two different kinds α and β of oxygen species, the former ("suprafacial") desorbing in the 300–600 °C temperature range and involved in soot combustion, the latter ("intrafacial") desorbing in the 600–900 °C range and involved in CFC of methane.

* Corresponding author. Tel.: +39 02 50314270; fax: +39 02 50314300.
E-mail address: cesare.oliva@unimi.it (C. Oliva).

1381-1169/$ – see front matter © 2005 Elsevier B.V. All rights reserved.
doi:10.1016/j.molcata.2005.09.037

The aim of the present work was then to investigate how the catalytic activity for the CFC of methane is affected by the partial substitution of Sr^{2+} with ions possessing a stable different oxidation state. In other words, our aim was to extend to other perovskitic catalysts the study of the effect of partial substitution of M^{2+} ions by ions with different valence, supporting this investigation by a deeper characterisation of the oxygen species through EPR analysis.

2. Experimental

2.1. Catalysts preparation

A detailed description of the FH apparatus can be found elsewhere [2]. Briefly, a H_2/O_2 flame is used, in which a clear precursors' aqueous solution is nebulised. The nano-size particles so formed are collected by means of an electrostatic precipitator. A temperature of nearly 1600 °C is attained by the flame in the region of particle formation. The high temperature and low residence time of the reagents in the flame guarantees a relatively high surface area and a very high thermal stability of the material.

2.2. Preparation of the solutions for FH and SGC preparation

2.2.1. FH samples: $Sr_{0.9}Gd_{0.1}TiO_{3\pm\delta}$ (GFH) and $Sr_{0.9}K_{0.1}TiO_{3\pm\delta}$ (KFH)

Eight grams of titanium iso-propoxide (Fluka, "purum") were dropped under vigorous stirring in 50 cm^3 of distilled water, to obtain a fresh titanium oxide ($TiO_2{\cdot}nH_2O$) suspension. Then 1.5 mol excess of citric acid was added to the solution, together with ca. 1 vol.% of 30 wt.% aqueous H_2O_2 solution, so to obtain the complete dissolution of the solid through complexation. The solution so obtained was mixed with another solution (total volume 10 cm^3) containing the stoichiometric amount of Sr-acetate (Aldrich, ≥99.995% pure) and of either $Gd(NO_3)_3$ (Aldrich, ≥99.99% pure) or of K-acetate (Aldrich, ≥99.9% pure) and citric acid (citric acid:Ti molar ratio = 0.5:1). The excess water was finally removed in rotavapor, till 100 cm^3 residual volume [6].

2.2.2. SGC samples: $Sr_{0.9}Gd_{0.1}TiO_{3\pm\delta}$ (GSG) and $Sr_{0.9}K_{0.1}TiO_{3\pm\delta}$ (KSG)

The solutions used for the FH samples have been employed also for the SGC ones. The only difference was the removing of water to dryness in rotavapor, till the formation of the solid. The latter was then calcined in flowing air, by increasing temperature by 0.5 °C/min up to 200 °C, then by 1 °C/min up to 850 °C, kept for 1 h (KSG) or 5 h (GSG).

2.3. Catalysts characterisation

BET specific surface area (BET_{SSA}) and porosity were determined by means of a Micromeritics ASAP 2010 instrument. XRD analysis was carried out by a Philips PW1820 powder diffractometer, using the Ni-filtered Cu Kα radiation (λ = 0.15418 nm). Shape and size of the particles were determined by means of a Cambridge Stereoscan 150 scanning electron microscope (SEM). X-band EPR spectra were collected by means of a Bruker Elexsys instrument, equipped with an ER4102ST standard rectangular cavity and with a cryostatic ancillary apparatus. The magnetic field intensity was accurately checked by an ER035M Bruker Teslameter and the microwave frequency was measured by a HP 5340A frequency counter. The Q-band (34 GHz) measurements were performed with a Bruker ESP300 E spectrometer equipped with a Q-band bridge and an ER5106QT cavity. The instrumental parameters were: 1 mW microwave power and 1 and 2 G modulation amplitude at 97 K and room temperature, respectively. The EPR spectra have been simulated by Bruker SimFonia and by SimEPR32 [7] simulation programmes.

2.4. Catalytic activity tests

Activity tests for the CFC of methane have been carried out by means of a bench-scale continuous apparatus. The catalyst (0.2 g), pelletised and then ground and sieved to 60–100 mesh particles, was mixed with 1.3 g of quartz particles of the same size and loaded into a vertical down-flow tubular quartz reactor, 7 mm i.d. The catalyst was kept in the isothermal central part of the reactor by means of quartz wool flocks. The empty parts of the reactor, above and below the catalyst, were filled with quartz beads (10–20 mesh). Reactant gases flow rates were controlled by means of MKS mod. 1259 mass flow regulators governed by a MKS 470 unit. The reactor was heated by an electric furnace, regulated by an Eurotherm mod. 812 TRC. The outlet gas was analysed in-line by means of an HP 5890A HWD gas chromatograph, equipped with Porapak Q and MS 5A columns. Before the reaction the catalyst was activated in situ in flowing air (20 cm^3/min), while increasing temperature by 10 °C/min up to 600 °C, kept for 1 h. The activity tests were carried out by feeding a gas mixture composed of 10 cm^3/min of 1.04% methane in helium and 10 cm^3/min of air, while increasing temperature by 2 °C/min from 250 to 650 °C.

3. Results

3.1. Catalysts characterisation by BET, XRD and SEM

BET_{SSA} was about 10 m^2/g for GFH, 2 m^2/g for GSG and ca. 5 m^2/g for both KFH and KSG samples. GSG showed the lowest surface area because it needed a 5 h heating at 850 °C (vide supra) to obtain the perovskite structure. These conditions caused the partial sintering of the catalyst particles. XRD analysis (Fig. 1) showed crystalline perovskitic structure for all the samples, accompanied for KSG by some $SrCO_3$ (characteristic reflections of the latter at $2\theta = 25.17°$, 25.80°, 36.53°, 44.08° [8]). The samples obtained by FH showed a higher crystallinity and phase purity with respect to the same samples prepared by the SGC technique. The better phase purity of GSG was due to the longer calcination time. Crystal size was calculated by applying, to the main five reflections of the XRD pattern, the

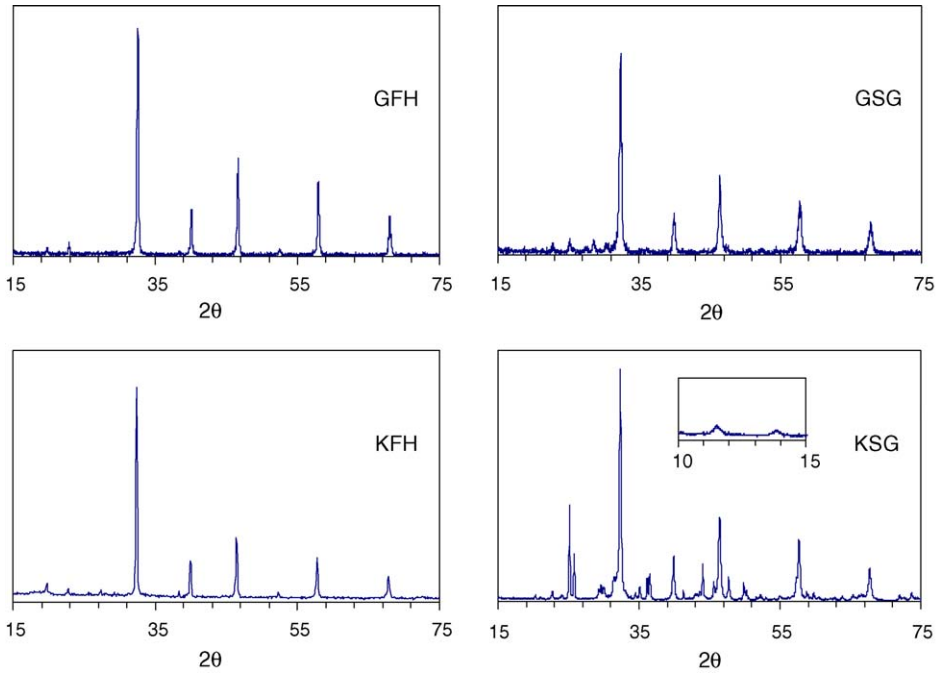

Fig. 1. XRD patterns.

Scherrer's equation [9]:

$$D = \frac{0.9 \times \lambda \times 180}{(B \times \cos\theta) \times \pi \times 10} \quad (1)$$

where $B = (\mathrm{FWHM}^2 - 0.15^2)^{1/2}$, D = diameter of crystal (nm), $\lambda = 1.5418$ Å = wavelength of the X-ray source, FWHM = width at half-height of the peak, θ = diffraction angle and $180/\pi$ = correlation factor. The parameters obtained are collected in Table 1. SEM analysis (Fig. 2) showed for GFH, GSG and KFH relatively uniform, nearly spherical particles, 50–300 nm in size for GFH, 50–400 nm for GSG and 100–250 nm for KFH. KSG showed a totally different aspect and a much-sintered structure.

3.2. X-band and Q-band EPR spectra

3.2.1. EPR spectra of $Sr_{0.9}Gd_{0.1}TiO_{3\pm\delta}$ (GFH)

The X-band EPR spectrum of GFH showed a high-intensity, nearly symmetric band at room temperature (Fig. 3). With decreasing temperature, this feature broadened and its intensity increased, though less than expected on the base of the Curie's law, while the presence of bumps like *B* was becoming more evident on the left part of the spectrum (Fig. 4). *B* became a bit more pronounced after the outgassing (10^{-2} mbar and 300 °C) preceding the BET analysis of the sample, whilst they completely disappeared after treating the sample with air at 600 °C for 1 h. By contrast, the spectral shape did not change significantly after catalytic use of GFH for CFC of methane, though the overall spectral intensity decreased. A more symmetric spectrum was obtained by Q-band EPR. At room temperature (Fig. 3) it was almost perfectly fitting the sum of two Lorentzian lines at $g = 1.991$ and 2.020, with a width of 604 and 1600 G, respectively, the former line corresponding to a species four times more concentrated than the latter. At 100 K these two lines changed a bit, assuming $g = 1.990$ and 2.010, with a width of 671 and 2160 G, respectively, the former corresponding to a species 1.5 times more concentrated than the latter (spectra here not shown).

Table 1
Crystal size and BET specific surface area of the examined samples

Sample	Crystal size[a] (nm)	BET_{SSA} (m^2/g)
$Sr_{0.9}K_{0.1}TiO_{3\pm\delta}$ (KFH)	29	5
$Sr_{0.9}K_{0.1}TiO_{3\pm\delta}$ (KSG)	61	5
$Sr_{0.9}Gd_{0.1}TiO_{3\pm\delta}$ (GFH)	56	10
$Sr_{0.9}Gd_{0.1}TiO_{3\pm\delta}$ (GSG)	24	2

[a] Calculated by the Scherrer equation.

3.2.2. EPR spectra of $Sr_{0.9}Gd_{0.1}TiO_{3\pm\delta}$ (GSG)

Both X-band and Q-band EPR spectra of fresh GSG at room temperature were composed of a single nearly symmetric feature at $g = 1.991$, with a peak-to-peak width of ca. 40 G (Fig. 5), i.e. less than 1/10 that observed with GFH (Fig. 3). With decreasing temperature, the intensity of these GSG spectra decreased a bit, while a second broader overlapping feature appeared both in X-band and Q-band (Fig. 6) spectra.

3.2.3. EPR spectra of $Sr_{0.9}K_{0.1}TiO_{3\pm\delta}$ (KFH)

A completely different feature was recorded with KFH, both with X-band and Q-band EPR. Indeed, this spectrum (Fig. 7) was composed of a very narrow Lorentzian-shaped line at $g \cong 2.008$, with temperature-independent peak-to-peak width $\Delta H_{pp} = 1.6$ G (X-band) and 3.4 G (Q-band). As shown in Fig. 8, this pattern was characterised by intensity (but not shape) comparable to that observed with pure $SrTiO_{3\pm\delta}$ prepared by the same FH procedure (Sample T2 of [3]). By contrast, this inten-

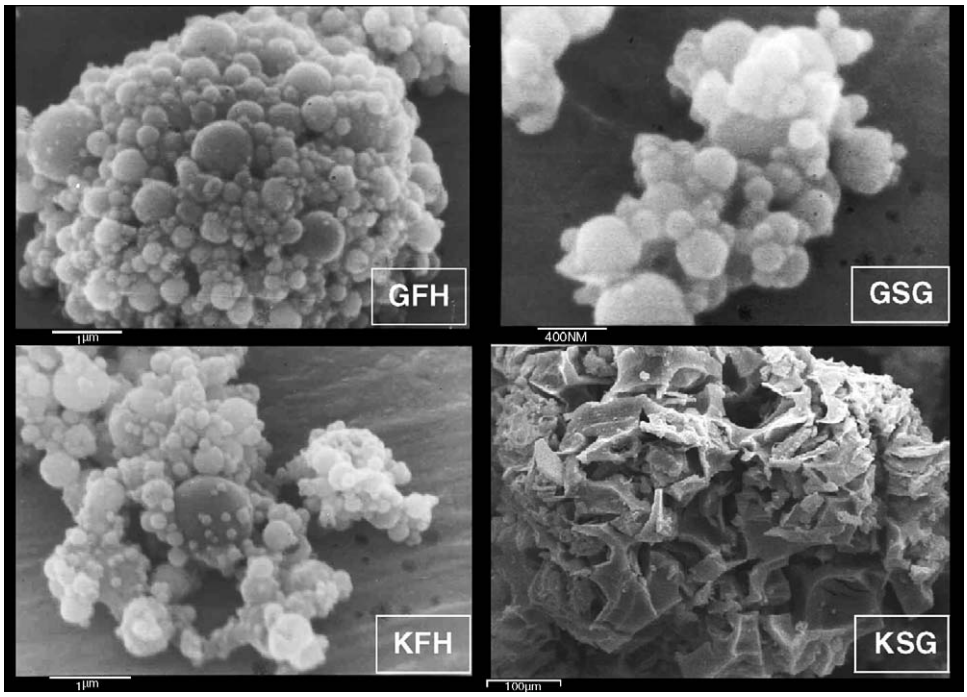

Fig. 2. Typical SEM images.

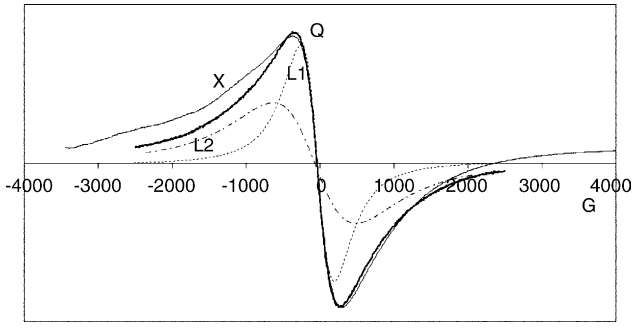

Fig. 3. Room temperature EPR spectra of GFH sample. X-band (thinner track) and Q-band (thicker track) experimental patterns. L1 and L2 (dotted tracks) are two Lorentzian-shaped lines simulating the Q-band EPR line.

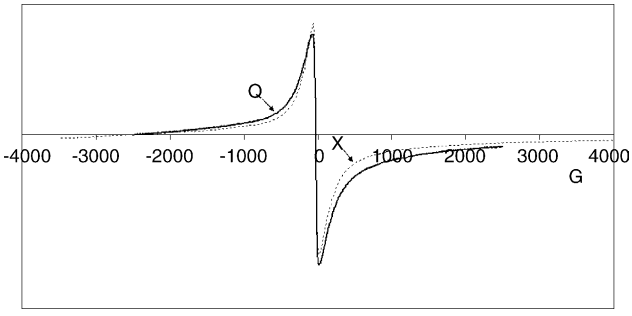

Fig. 5. Room temperature Q-band (thicker track) and X-band (dotted track) EPR spectra of GSG sample.

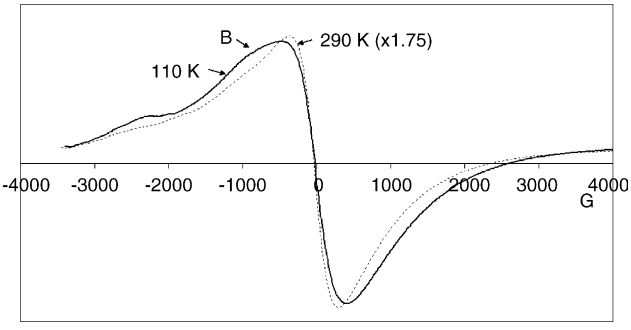

Fig. 4. X-band EPR spectra of GFH sample, recorded at 110 (thicker track) and 290 K (dotted track, multiplication factor 1.75).

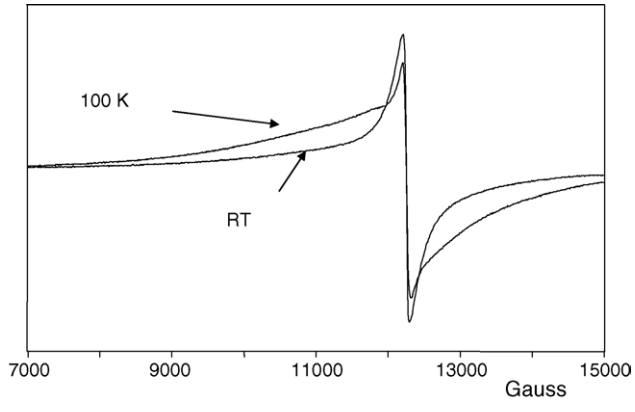

Fig. 6. Q-band EPR spectra of GSG sample, recorded at two different temperatures.

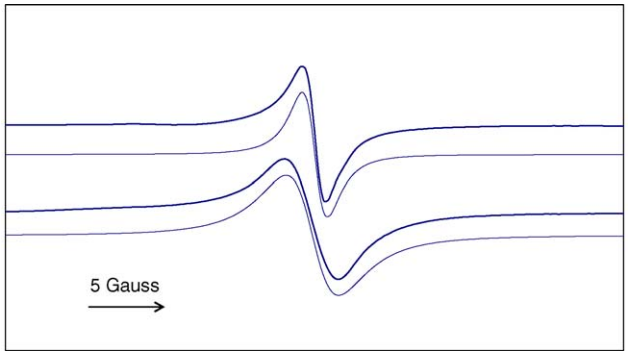

Fig. 7. X-band (upper) and Q-band (lower) EPR spectra of KFH sample, recorded at 290 K. The thinner lines are Lorentzian-shaped simulations.

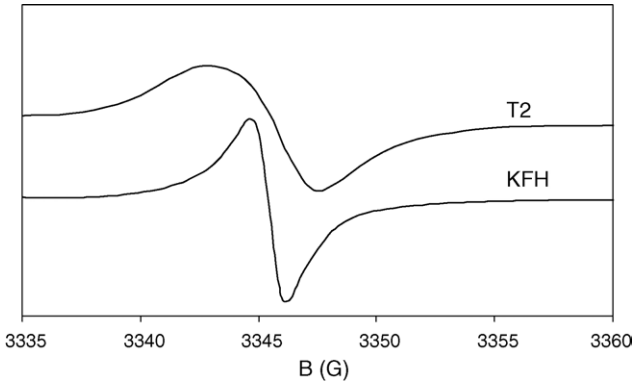

Fig. 8. X-band EPR spectra of KFH and T2 samples, recorded at 140 K.

sity was by far lower than that of the broad features above reported with GFH and GSG; therefore, we cannot exclude its presence also with those samples, masked by their main spectral feature. Furthermore, this pattern disappeared after catalytic use of KFH.

3.2.4. EPR spectra of $Sr_{0.9}K_{0.1}TiO_{3\pm\delta}$ (KSG)

No EPR signal at all was observable with fresh KSG sample. However, sometimes a low-field broad band, becoming more intense with decreasing temperature, appeared after catalytic use (Fig. 9). When this was the case, the intensity of this feature was strongly reduced by carrying on a deeper oxidation of the

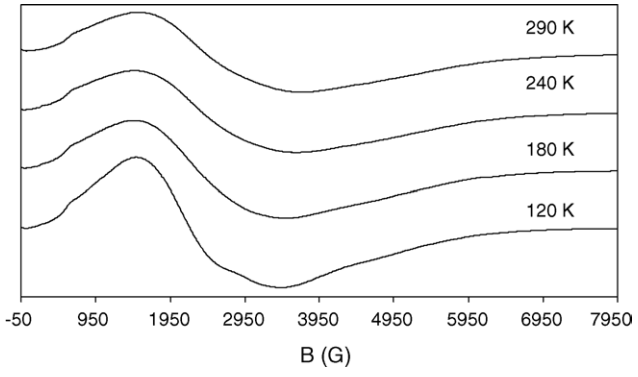

Fig. 9. X-band EPR spectra of a KSG sample, after catalytic use for the CFC of methane. Recording temperatures ranging between 120 (bottom) and 290 K (top).

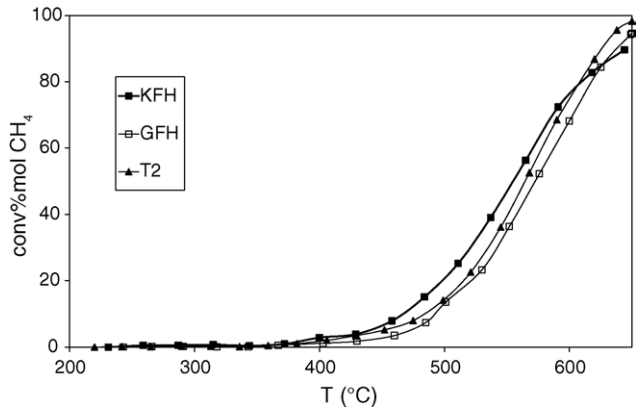

Fig. 10. Comparison of the activity of KFH, GFH and T2 catalysts for the CFC of methane.

sample. For example, the R.T. spectrum of Fig. 9 reduced to about 1/10 after sample oxidation in air at 600 °C for 1 h, while its maximum moved by about 490 G towards higher field values. The only titanate sample showing this kind of spectrum was the undoped $SrTiO_{3\pm\delta}$ prepared by the sol–gel (SG) method (Sample T3 of [3]) after use as catalyst for CFC of methane (spectrum here not shown).

3.3. Activity tests for the CFC of methane

In-line analysis of the gas coming out from the methane CFC reactor was made every 10 min. Some results are collected in Fig. 10 as mol% conversion of methane versus temperature. KFH was the most active catalyst until ca. 600 °C. At higher temperature GFH was more active than KFH, though pure $SrTiO_{3\pm\delta}$ (Sample T2 of [3]) showed the best catalytic performance. KSG and especially GSG showed the worst catalytic activities at any investigated temperature (not reported).

4. Discussion

The EPR spectra observed with the four examined samples are surprisingly different from each other, depending both on chemical composition and preparation method. The great intensity and the spectral shape of the broad X-band spectrum reported at room temperature with GFH (Fig. 3) can be safely attributed to ferromagnetic (FM) resonance of Gd^{3+} ion domains. In particular bumps like *B* (more accentuated at lower temperatures, Fig. 4) indicate the presence of internal magnetic fields in FM systems with positive axial anisotropy [10]. Furthermore, the spectral intensity of this pattern decreases at higher temperature by far less than expected on the base of the Curie's Law, indicating that the single ions are indeed reciprocally interacting in a ferromagnetic way. The Q-band spectrum of the same GFH sample appears more symmetric, and composed (vide supra) by two overlapping Lorentzian lines (Fig. 3), 604 and 1600 G broad, respectively, at room temperature, both broadening with decreasing temperature. The presence of bumps like *B* in the X-band spectrum, and not in the Q-band, further confirms their attribution to FM systems with

magnetic anisotropy $\Delta H_a \equiv |H_\parallel - H_\perp|$, where: ΔH_a = magnetic anisotropy (as defined in the text), $H_\parallel = H$ parallel, $H_\perp = H$ perpendicular. Indeed, the following equation holds [10]:

$$\Delta H_a = \alpha' \frac{\nu_Q \Delta H_{pp}(X) - \nu_X \Delta H_{pp}(Q)}{\nu_Q - \nu_X} \quad (2)$$

where $\alpha' = 1.732$ for Lorentzian shape. Since $\Delta H_a \geq 0$, Eq. (2) requires $\Delta H_{pp}(X) \geq 1/3\ \Delta H_{pp}(Q)$, as in this case, where $\Delta H_{pp}(X) > \Delta H_{pp}(Q)$. However, no reliable quantitative evaluation of the magnetic anisotropy ΔH_a (GFH) can be obtained, due to the low spectral resolution (Fig. 3).

Furthermore, the presence of FM systems is also in-line with the observed intensity variation of structures like *B* upon reducing/oxidising treatments. Indeed, any reducing process, even the vacuum pumping before BET analysis, limits super-exchange interactions among Gd^{3+} ions through bridging oxygen, favouring instead a direct ferromagnetic interaction among them.

As for the GSG sample, the intensity of the narrow X-band and Q-band (Fig. 5) is not increasing at all with decreasing temperature, as it should be on the base of the Curie's law, but, on the contrary, it decreases a bit, while a second broader overlapping pattern appears. This behaviour is in accordance with the particle nanometric size of this sample. In fact, it has been reported [10] that with small (single-domain) particles (as it is the case with GSG, with particle diameter of ca. 20 nm, Table 1) the FM resonance bands contribute to broad features like that of Fig. 6 at low temperature only. By contrast, at higher temperature, when *kT* overcomes the small anisotropy energy of these particles, the FM resonance bands narrow and merge into a Lorentzian-shaped (superparamagnetic, SPM) line, similar to the symmetric narrow feature of Fig. 6. At intermediate temperatures an intermediate regime must occur in these systems, in which a "two-line pattern" as that of GSG at 100 K (Fig. 6) appears, formed of a broad feature overlapping a narrower one [11–14]. The relative intensity of these two spectral contributions depends on particle size and shape distribution function, as well as on the magnitude of the magnetic anisotropy.

In any case, these FM (or SPM) species formed with GFH and GSG samples seem not much involved in the present catalytic reaction. Indeed, only a small decrease of their spectral intensity was noticed, while their spectral profile did not change significantly, after the use of these catalysts for the present reaction.

A completely different situation can be sketched for the $Sr_{0.9}K_{0.1}TiO_{3\pm\delta}$ sample. Indeed, the partial substitution of K^+ for Sr^{2+} could be counterbalanced both by a partial oxygen deficiency (i.e. a negative sign in front of δ) and/or a partial oxidation of Ti^{3+} to Ti^{4+}. However, the last is confirmed by the EPR spectra of KFH (Figs. 7 and 8), the single line at $g \cong 2.008$ being attributable to Ti^{4+}/O_3^- [3,15–17]. Indeed, an EPR feature with *g* components 2.011, 2.008 and 2.002 has been attributed to O_3^- ions adsorbed on titania surfaces [18] and to O_2^- adsorbed on other solid systems [19–22] and in most cases such ions were characterised by high mobility ("suprafacial" α oxygen). The apparently a bit broader line recorded with KFH at higher microwave frequency (Fig. 7) should be due to the higher spectral resolution of the Zeeman spectral components, obtained by the Q-band EPR analysis with respect to X-band.

The disappearing of this line after catalytic use indicates that the corresponding paramagnetic species is involved in the reaction, i.e. it is very likely a surface species. A comparison between KFH and the corresponding $SrTiO_{3\pm\delta}$ sample prepared by the same FH method (labelled with T2 in [3]) confirms this attribution. The EPR spectra of these two samples (Fig. 8) have the same mean *g* value (at room temperature), nearly the same (low) intensity, but a different shape. The broad and asymmetric line of T2 is due to paramagnetic species not completely free to move on the surface of the catalyst. By contrast, the narrow and symmetric line of KFH suggests that the same paramagnetic species are almost free to move, mixing their magnetic Zeeman anisotropies and, therefore, showing a "motional narrowed" Lorentzian-shaped spectrum due to free tumbling of the O-based radical species on the solid surface. Indeed, *g* tensor anisotropies of 1×10^{-3} (corresponding to Q-band Zeeman energy anisotropies of 10^{-26} J) were resolved for T2 sample [3] by Q-band EPR at low temperature. These anisotropies, corresponding at 34 GHz (Q-band) to ca. 6 G, i.e. to 17 MHz, have not been resolved with the KFH sample in the present investigation. This means that the exchange frequency of anisotropy mixing must exceed 17 MHz with KFH, but not with T2. Thermal energy at 100 K corresponds to ca. 10^{-21} J and hence it largely overcomes the Zeeman energy anisotropy of these oxygen-based radicals: anisotropy features can be observed only if the radical species motion is frozen by the interaction with the catalyst surface, as it happens with T2 sample. On the other hand, the low temperature availability of almost free α oxygen on the KFH surface is in-line with the better activity of this catalyst with respect to the undoped T2 sample at lower temperature only (Fig. 10). At higher temperature KFH has lost its α surface oxygen, so becoming less active than T2 (Fig. 10).

At last, the low-field broad band, shown only by KSG (Fig. 9) and by $SrTiO_{3\pm\delta}$ (SG) (Sample T3 of [3]) after catalytic use, need a deeper discussion. A feature like this has been found by us [23] with a $La_{0.9}Sr_{0.1}CoO_3$ perovskitic sample, characterised by a relatively low catalytic activity for the CFC of methane, as KSG in the present paper and T3 in ref. [3]. This pattern is the typical low-field contribution to the FM spectrum of a system characterised by a strong uniaxial magnetic anisotropy. The low-field maximum and the high-field minimum of this kind of spectra are detected at H^+ and H^- magnetic field values, respectively, not related to the *g* tensor of the system but, instead, to the intensity of its magnetic anisotropy [10]. Systems like these can be due to spin bags of O^- [23–25], forming in incompletely re-oxidised perovskites. In fact, re-oxidation should proceed [26] as follows:

$$O_{2,g} \leftrightarrow O_{2,ads}{}^- + h^\bullet \quad (3)$$

$$O_{2,ads}{}^- \leftrightarrow O_{2,ads}{}^{2-} + h^\bullet \quad (4)$$

$$O_{2,ads}{}^{2-} \leftrightarrow 2O_{ads}{}^- \quad (5)$$

$$O_{ads}{}^- + V_O{}^{\bullet\bullet} \leftrightarrow O_O{}^X + h^\bullet \quad (6)$$

where $h^{\bullet}$ = hole, $V_O^{\bullet\bullet}$ = vacant oxygen site, O_O^X = (uncharged) oxygen on lattice site. It has also been reported that all catalysts show two re-oxidation regimes. The first one is accompanied by a low enthalpy change and is connected with the re-oxidation of surface vacancies. The second one corresponds to the re-oxidation of bulk oxygen vacancies and is characterised by a much higher enthalpy change, as well as by a marked dependence on structure and composition of the sample, greatly affecting the oxygen vacancy diffusion. Therefore, incomplete bulk vacancies re-oxidation would end at step (5), leaving a significant amount of O_{ads}^- in the sample, grouping into spin bags showing the FM resonance spectra of Fig. 9.

5. Conclusions

The partial substitution of Sr^{2+} in $SrTiO_3$ causes a worsening of the catalytic activity of the sample when the charge of the dopant ion is 3+, but an improvement, though only at lower temperature, when that charge is 1+. Indeed, in the former case the partial substitution with the trivalent Gd^{3+} ion forces Ti^{4+} to Ti^{3+}, which cannot take part any more in the CFC of methane. By contrast, the oxidation of Ti^{3+} to Ti^{4+}, forced by the partial substitution with the monovalent K^+ ion, favours the formation of the oxidant species Ti^{4+}/O_3^-. However, O_3^- ions appear almost free to move on the KFH surface ("suprafacial" oxygen species) as confirmed by their narrowed Lorentzian-shaped EPR line, observed even at 34 GHz microwave frequency (Q-band) EPR. By contrast, O_3^- species remain more firmly adsorbed on the surface of the undoped (T2) sample. Hence, KFH reveals a catalytic activity higher than T2 at $T < 550\,^{\circ}C$, possibly because of a higher availability of surface almost free (suprafacial) O_3^- species, which could favour a higher activity for soot combustion [5].

Acknowledgment

We are indebted to Professor A.V. Vishniakov for helpful discussion.

References

[1] M.F.M. Zwinkels, S.G. Järås, T.A. Griffin, Catal. Rev. Sci. Eng. 35 (1993) 319.
[2] L. Forni, I. Rossetti, Appl. Catal. B: Environ. 38 (2002) 29.
[3] C. Oliva, L. Bonoldi, S. Cappelli, L. Fabbrini, I. Rossetti, L. Forni, J. Mol. Catal. A: Chem. 226 (2005) 33.
[4] R.D. Shannon, Acta Crystallogr., Sect. A 32 (1976) 751.
[5] D. Fino, N. Russo, G. Saracco, V. Specchia, J. Catal. 217 (2003) 367.
[6] J. Garcia-Jaca, J.L. Pizarro, J.I.R. Larramendi, L. Lezama, M.I. Arriortua, T. Rojo, J. Mater. Chem. 5 (1995) 227.
[7] (a) A. Adamski, T. Spalek, Z. Sojka, Res. Chem. Intermed. 29 (2003) 793;
(b) T. Spałek, P. Pietrzyk, Z. Sojka, J. Chem. Inf. Model 45 (2005) 18.
[8] Selected Powder Diffraction Data, JCPDS, Swarthmore, PA (1974–1982), file 5–418.
[9] G. Strukul, F. Signoretto, Advanced Catalysts and Nanostructural Materials, Academic Press, New York, 1996, p. 160.
[10] L. Bonneviot, D. Olivier, in: B. Imelik, J.C. Védrine (Eds.), Catalyst Characterization. Physical Techniques for Solid Materials, Plenum Press, New York, 1994, p. 181.
[11] V.K. Sharma, F. Waldner, J. Appl. Phys. 48 (1977) 4298.
[12] Y.L. Raikher, V.I. Stepanov, Phys. Rev. B 50 (1994) 6250.
[13] R. Berger, J. Kliava, J.-C. Bissey, J. Appl. Phys. 87 (2000) 7389.
[14] Yu.A. Koksharov, D.A. Pankratov, S.P. Gubin, I.D. Kosobudsky, M. Beltran, Y. Khodorkovsky, A.M. Tishin, J. Appl. Phys. 89 (2001) 2293.
[15] P. Meriaudeau, J.C. Védrine, J. Chem. Soc., Faraday Trans. II 72 (1976) 472.
[16] A.R. Gonzalez-Elipe, G. Munuera, J. Soria, J. Chem. Soc., Faraday Trans. I 75 (1979) 748.
[17] Y. Takita, M. Iwamoto, J. Lunsford, J. Phys. Chem. 84 (1980) 1710.
[18] A.L. Attwood, D.M. Murphy, J.L. Edwards, T.A. Egerton, R.W. Harrison, Res. Chem. Intermed. 29 (2003) 449.
[19] R.F. Howe, W.C. Timmer, J. Chem. Phys. 85 (1986) 6129.
[20] A. Tuel, J. Diab, P. Gelin, M. Dufaux, J.-F. Dutel, Y. Ben Taarit, J. Mol. Catal. 63 (1990) 95.
[21] T. Yang, L. Feng, S. Shen, J. Catal. 145 (1994) 384.
[22] K. Dyrek, A. Adamski, Z. Sojka, Spectrochim. Acta A 54 (1998) 2337.
[23] C. Oliva, L. Forni, A.V. Vishniakov, Spectrochim. Acta A: Mol. Spectrosc. 56 (2000) 301.
[24] H. Thomann, R.A. Klemm, D.C. Johnston, P.J. Tindall, H. Jin, D.P. Goshorn, Phys. Rev. B 38 (1988) 6552.
[25] S. Khan, A. Singh, R.J. Singh, Solid State Commun. 106 (1998) 621.
[26] P.J. Gellings, H.J. Bouwmeester, Catal. Today 12 (1992) 1.